Soft Matter

Glassy Worm-Like Micelles in Solvent and Shear Mediated Shape Transitions

Journal:	*Soft Matter*
Manuscript ID	SM-ART-01-2018-000080.R1
Article Type:	Paper
Date Submitted by the Author:	30-Mar-2018
Complete List of Authors:	Chakraborty, Kaushik; City University of New York, College of Staten Island Vijayan, Kandaswamy; Plexium, Inc. Brown, Andre; Imperial College London Institute of Clinical Sciences Discher, Dennis; University of Pennsylvania, Laboratory for Research on the Structure of Matter Loverde, Sharon; City University of New York, College of Staten Island,

Journal Name

ARTICLE

Glassy Worm-Like Micelles in Solvent and Shear Mediated Shape Transitions

Kaushik Chakraborty[a], Kandaswamy Vijayan[b], Andre E. X. Brown[c], Dennis E. Discher[d], Sharon M. Loverde[a,e,f]

Received 00th January 20xx,
Accepted 00th January 20xx

DOI: 10.1039/x0xx00000x

www.rsc.org/

Glassiness of polymer melts is generally considered to be suppressed by small dimensions, added solvent, and heat. Here we suggest that glassiness persists at the nanoscale in worm-like micelles composed of amphiphilic diblock copolymers of poly(ethylene oxide)–polystyrene (PS). The glassiness of these worms is indicated by a lack of fluorescence recovery after photobleaching as well as microns-length rigid segments separated by hinges. Coarse-grained molecular dynamics studies probe the dynamics of the PS in these glassy worms. Addition of organic solvent promotes a transition from hinged to fully flexible worms and to spheres or vesicles. Simulation demonstrates two populations of organic solvent in the core of the micelle—a solvent 'pool' in the micelle core and a second population that accumulates at the interface between core and corona. Stable heterogeneity of residual solvent could explain the unusual hinged rigidity, but solvent removal during shear-extension could be more effective and yield - as observed - nearly straight worms without hinges.

A. Introduction

Amphiphilic copolymers with strongly segregating blocks readily form self-assembled structures in water spanning similar morphologies as found in their small-molecule surfactant counterparts[1-3]. Worm micelles are a novel class of stable with tunable-property self-assembling macromolecules and have an enormous potential for drug delivery[4-6] and bio-nanotechnology[7, 8]. Most of the worm micelles that have been studied so far have fluid phase hydrophobic cores, or contain solvent additives that fluidize the core, rendering the worms flexible[8-10]. However, there are some exceptions[11]. For example, rigid worm-like micelles have been found for the case of worm-micelles with the hydrophobic block composed by semi-crystalline polycaprolactone[11]. Herein we demonstrate that polystyrene-based copolymers, in addition to polycaprolactone-based copolymers, can be utilized to engineer worm-like micelles with controlled rigidity. Extreme hydrophobicity and a high glass transition temperature (around 100 °C) make polystyrene-based worm-like micelles a unique case to study glassiness at the nano-scale. Surface and interfacial effects on the glass transition temperature and associated structural relaxation is a widely debated issue[12-16]. Previous experiments on thin films of polystyrene (PS) consistently show a decrease in glass transition temperature as the film width is decreased[13, 16, 17]. Similar results have been found for polystyrene nanoparticles [18-22] and micelles[23, 24]. Experimental studies on polystyrene-based micellar aggregates have also characterized morphological transitions[9, 25-27] between phases as a function of block-specific solvents, as well as on the rheology of aggregates of micelles. Indeed, diblock copolymer assemblies that exhibit order-order transitions such as vesicle-to-worm[28], vesicle-to-sphere[29], or even vesicle-to-polymersomes[30] are of interest as stimuli-responsive materials [31]. The free energy of the micelle system with encapsulated hydrophobic solvent has multiple contributions: the entropic and enthalpic mixing contributions of the hydrophobic polymer with the organic solvent, the entropic and enthalpic contributions of the hydrophobic polymer with respect to water, the deformation of the hydrophobic and hydrophilic polymers, the entropic and enthalpic contributions due to swelling of the hydrophilic block, the entropic cost to localize the polymer to the interface, as well as the interfacial tension[32]. Herein we characterize morphological transitions of glassy worm-like micelles through incorporation of organic solvent in the micellar core with coarse-grained simulations of PEO-PS worm-like micelles that complement macroscopic observations of their contour length and flexibility, demonstrating a transition from worm-to-sphere.

The glass transition of polymer melts has been characterized computationally most extensively with the Kremer-Grest bead-spring model[33]. Recently, this model has been used to study the effects of nano-confinement on the glass transition in confined polymer layers[34]. Bead-spring models have also been used to study the effects of aging on the glass transition temperature in freely standing films[35]. Polystyrene has been increasingly well-studied with simulation techniques[36-42]. Numerous molecular-based models for PS have been developed, utilizing both structural[40] and thermodynamic[43] mapping methodologies. Indeed, these types of approaches to coarse grain force field development have shown to be fairly transferrable and applicable to the simulation of a range of soft self-assemblies[41, 43-49]. Within this study, we expand a previously developed Shinoda-DeVane-Klein (SDK)-type model of

[a] 1Department of Chemistry, College of Staten Island, The City University of New York, 2800 Victory Boulevard, Staten Island, New York, 10314 U.S.A.
[b] 2Plexium, Inc.
[c] 3Institute of Clinical Sciences, Faculty of Medicine, Imperial College London, London, UK
[d] 4Department of Chemical and Biomolecular Engineering, University of Pennsylvania, Philadelphia, PA 19104 U.S.A.
[e] 5Ph.D. Program in Chemistry, The Graduate Center of the City University of New York, New York, NY, 10016 U.S.A.
[f] 6Ph.D. Program in Physics, The Graduate Center of the City University of New York, New York, NY, 10016 U.S.A.

polystyrene[41], and combine it with an SDK coarse grain model of polyethelene-oxide[44] to simulate PEO-PS diblock copolymer worm-like micelles in solution. These simulations add molecular level insight to macroscopic observations of these glassy worms.

Herein we study the PEO-PS system on the scale of the individual worm molecules, and directly visualize worm dynamics and solvent effects using fluorescence microscopy. We also perform molecular dynamics simulations (MD) of 0.3 micron long PEO-PS worm micelles both in aqueous medium for 0.7 microsecond simulations and in the presence of a model organic solvent. We computationally characterize polymer segmental relaxation within the worm micelles, and demonstrate a decrease in relaxation time of the PS as a function of incorporated organic solvent concentration. This correlates with a decrease in contour length as well as a shift in morphology observed at the macro-scale. Within the worm micelle, we find that organic solvent accumulates both at the hydrophobic/hydrophilic interface and also in the center of the worm micelle core. As a function of increased concentration of organic solvent, the pool of organic solvent accumulates in the center of the hydrophobic core with an increasing entropic contribution compared to solvent that accumulates at the hydrophobic/hydrophilic interface that would correspond to a decrease the interfacial tension between the core and corona. In addition to the organic solvent that accumulates in the center of the micelle core, we find that the radius of the core increases, the width of the hydrophobic/hydrophilic interface increases, and the volume fraction of hydrophobic polystyrene decreases as a function of increased hydrophobic solvent concentration. Thus, there is a change in the dilution of the PS which likely gives rise to a shift in the enthalpic and entropic mixing free energy of the PS as a function of increased solvent concentration[32].

B. Materials and Methods

In brief, experiments were performed with PS-PEO of varying molecular weights OS30 (PEO_{56}-PS_{28}, M_n 5.5 kg/mol) and OS90 (PEO_{193}-PS_{86}, M_n 17.5 kg/mol). Worm micelles were prepared by the co-solvent evaporation method. The cores of the micelles were labeled by 1 µL hydrophobic fluorophore PKH26 to enable visualization under fluorescence microscopy. Like experiment, two different PEO-PS worm-like micelles with chain lengths of $PEO_{56}PS_{28}$ (OS30) and $PEO_{70}PS_{31}$ (OS31) were simulated using LAMMPS[50]. Snapshot of the equilibrated OS30 worm micelle is shown in **Figure 1A and 1B**. **Figure 1A and 1B** are the same snapshot of the worm micelle from two different angles to show the core and corona more clearly. Each system contained approximately 1200 polymers and 400,000 water molecules. The total system size is nearly 800,000 coarse grain beads with box dimensions of approximately 0.3 x 0.3 x 0.5 µm. Both 0.3 micron long OS30 and OS31 worms were simulated for 700 ns with the time step of 10 fs. All simulations were performed under NPT conditions at 300 K. To explore the effect of solvent, we performed four additional simulations of OS30 in the presence of 2.5%, 5%, 10%, and 20% model hydrophobic solvent. In these cases, we inserted 3250, 6500, 13000, and 26000 hydrophobic beads randomly inside the core of the worm. This is followed by 50 ns simulation of each of the system under NPT ensemble conditions following the same protocol as described above. Additional experimental and simulation methods are available in the **Supplemental Information**.

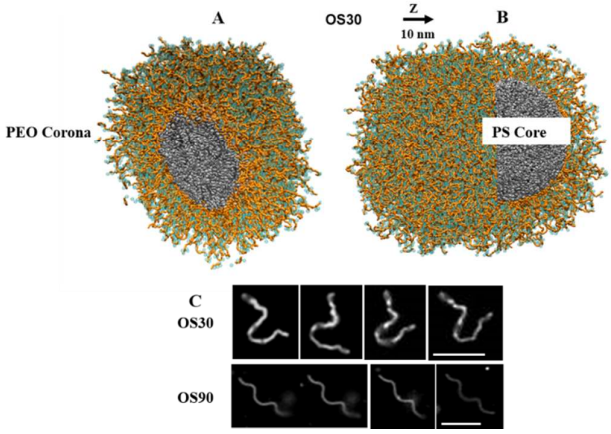

Fig 1 (A) Snapshot of OS30 worm micelle after 0.7 microseconds from one end removing the endcap to show the orange PEO chains and glassy PS core in grey. CG water beads within 5 Å of the PEO is shown in cyan. (B) Side view of OS30 worm micelle with same coloring scheme, removing a portion of the hydrophilic PEO to show the PS core. (C) Snapshots of an OS30 and an OS90 worm. Snapshots are 1-2 sec between frames. The hinged motion of the OS30 worm is clearly visible compared to the extremely rigid whole body motion of the OS90 worm. Scale bar 10

C. Methodology

Dynamical properties of PEO and PS were investigated by calculation self-intermediate scattering function (F_s *(Q,t)*). F_s *(Q,t)* can be represent as

$$F_s(Q,t) = < \exp(-iQ(\mathbf{r_i}(t) - \mathbf{r_i}(0)) >$$

where *Q* is the wave vector, and $r_i(t)$ and $r_i(0)$ denote position vectors of the *i*-th tagged bead at time *t* and *t* = 0, respectively. The value of |*Q*| is taken to be 1 $Å^{-1}$ in the calculations.

Thermodynamic properties of the hydrophobic solvent were then calculated using SPAM method [51]. According to this method, the free energy of a solvent can be represent as

$$\boldsymbol{G_{SPAM}} = -\boldsymbol{RT\ lnQ_{SPAM}} \quad (1)$$

$$\boldsymbol{Q_{SPAM}} = \sum_{E_S}[\boldsymbol{P(E_S)}\ \mathbf{exp}(-\tfrac{\boldsymbol{E_S}}{\boldsymbol{RT}})] \quad (2)$$

where $\boldsymbol{Q_{SPAM}}$ is the partition function and *P* (E_S) is the probability of a solvent having interaction energy E_S with its surroundings. Then, the enthalpic component ($\boldsymbol{S_S}$) can be calculated using Equation 3

$$\boldsymbol{TS_S} = < \boldsymbol{E_S} > - \boldsymbol{G_{SPAM}} \quad (3)$$

where $<E_s>$ is the average energy of the solvent. The interaction energy of the solvent was calculated by computing the non-bonded energy of a tagged solvent with its surrounding. Here, we explored the thermodynamic properties of the solvent as a function of distance from the central axis of the worm. To calculate the position dependent thermodynamic properties of the hydrophobic solvent, we divided the whole volume of the worm micelle with equally spaced bins with radius of approximately 10 Å and then

calculated the corresponding energy probability distributions $P(E_s)$ for each bin separately.

All calculations such as: *i)* density profiles, *ii)* core radius *iii)* self-intermediate scattering function *iv)* mean square displacements were performed over last 600 ns of equilibrated trajectories. For mean square displacement and self-intermediate scattering function, we performed block-averaging. We split each 600 ns trajectory into 4 blocks, where each block consists of 150 ns duration. In presence of model hydrophobic solvent, last 40 ns trajectories were used for all the calculations. Thermodynamic properties of hydrophobic solvent were also calculated using block average. We split each 40 ns trajectory into 4 different blocks with 10 ns duration.

D. Results and Discussion Extreme hydrophobicity and a high glass transition temperature make polystyrene-based worm-like micelles an ideal case to study glassiness at the nano-scale. Furthermore, the presence of the hydrophilic corona along with the hydrophobic core makes these systems even more interesting. Herein, first we characterize the structure and glassiness of the PS-PEO worm micelle. Data suggests extremely glassiness of the worm core even at high temperatures. The glassy nature of the PS core also makes the worm very rigid over a range of temperatures. While temperature has very little effect, hydrophobic solvent easily breaks the glassiness of the core and changes the rigidity as well as shape of the worm micelle. Computer simulations allow us to explore the dynamics of worm core and corona separately, as well as the shift in organic solvent partitioning as a function of increased solvent concentration. These studies may provide important insight about the shape change of the diblock copolymer assemblies in the presence of small guest molecules.

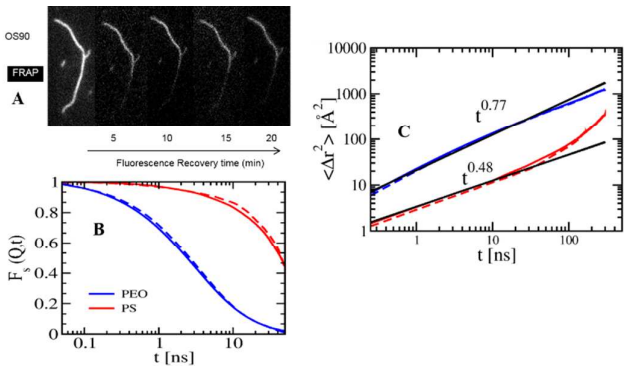

Fig 3 (A) Fluorescence recovery time of OS90. (B) Self intermediate scattering function, $F_s(Q,t)$, and (C) MSD of center-of-mass of the PEO and PS chains. Here solid and dotted lines represents data for OS30 and OS31 respectively.

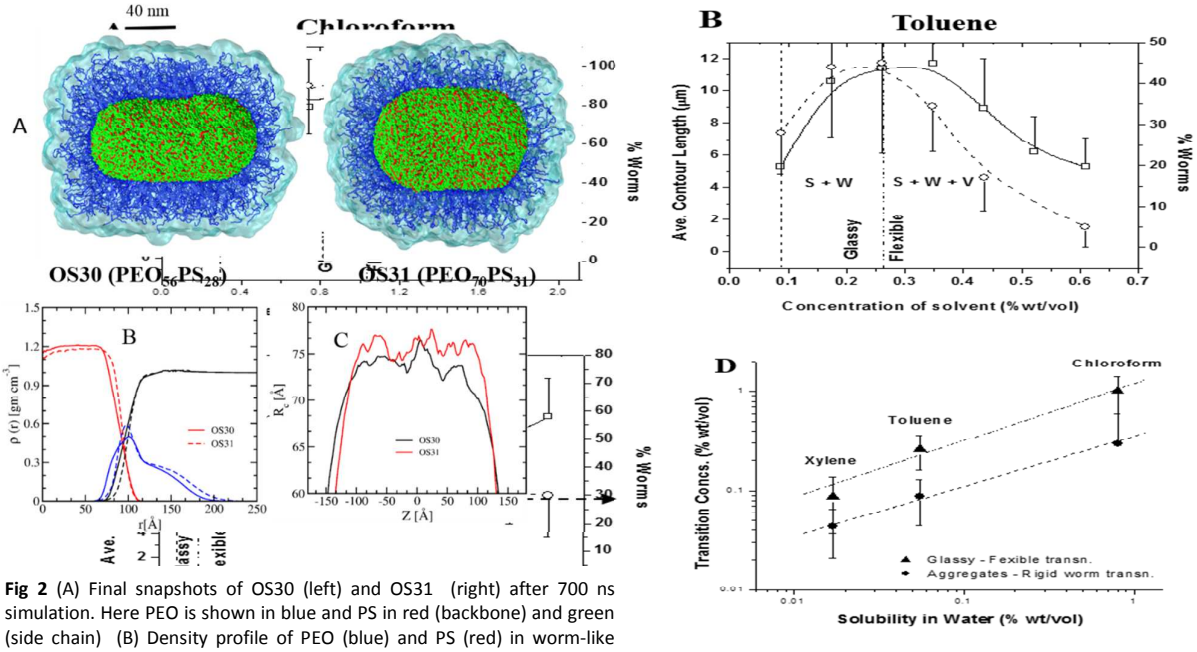

Fig 2 (A) Final snapshots of OS30 (left) and OS31 (right) after 700 ns simulation. Here PEO is shown in blue and PS in red (backbone) and green (side chain) (B) Density profile of PEO (blue) and PS (red) in worm-like morphology relative to the center of mass of the worm core. Density of water is shown in black. Data for OS30 and OS31 are shown in solid and dotted lines respectively. (C) Average radius of the core along the central axis of the worm averaged over 600 ns trajectories. ıstant in the solution for a wide range of solvent concentrations (A) worm, sphere and vesicle respectively. (D) The solubilities of the the concentrations at which worms are induced and the glassy to flexible transition.

Structure and Glassiness Polystyrene is a glassy polymer with a glass transition temperature for bulk systems close to 100 C [13]. Both the OS30 and OS90 diblock systems have a hydrophilic to hydrophobic polymer ratio that is conducive to forming cylindrical micelles, and thus at room temperature they are expected to from worm micelles that exhibit some form of glassiness. Due to the extreme hydrophobicity of polystyrene, hydrating thin films of PEO-PS result in precipitation and large aggregate formation. To overcome this, the co-solvent evaporation method is used. The presence of a suitable solvent for polystyrene ensures substantial fluidity in the hydrophobic region to form nominal structures. Evaporating out the solvent can then lock in these structures. Upon complete co-solvent evaporation, the aqueous solutions of low molecular weight OS30 copolymer are found to form stiff, convoluted worm like micelles as shown in **Figure 1C** with an average contour length of around 12μm +/-.6μm. The average core diameter of OS30 worms is found to be 15 nm from AFM measurements, while OS90 worms are 30 μm +/- 12 μm in contour length with a core diameter of about 30 nm. The thicker core most likely strengthens the worm backbone enabling OS90 to have much longer contour lengths without breaking. The dynamics of the worm motion is characterized by fluctuations about hinges along an otherwise rigid and jagged backbone. Except for the fluctuations about the hinges, the worms predominantly exhibit rigid whole-body motion (**Figure 1C**). Further information is in **SI-1** characterizing the distance and angles between hinges.

Simulation snapshots of both OS30 and OS31 worm micelles after 700 ns are shown in **Figure 2A**. The hydrophobic PS core is very stable but the PEO corona is loose and brushy. A similar loose and brushy PEO corona is also observed in previous simulation studies of PEO-PCL worm micelles[52]. Unlike experiment, the simulated worm micelles have no 'hinges' along the rigid backbone. The difference in lengths of the worm-micelles between the experimental (~10 micron) and the simulated (~ 400 Å) worms may be responsible for this. Next, to explore the distributions of hydrophobic and hydrophilic monomer in the worm-like morphology in more detail, in **Figure 2B**, we present the density profile of PEO, PS, and water as a function of distance from the central axis of the micelle. Density profiles reveal that the micellar cores are mainly composed of hydrophobic PS molecules. The average radius of the worm core is around 70 Å (width of the plateau region of the PS density profile). This agrees very well with the experimentally estimated average diameter (150 Å) of OS30 from AFM measurements. The density of the PS in the core of the micelle ~ 1.1 g/cm^3, which is slightly higher than the reported bulk PS density of 1.04 g/cm^3. The relatively broader distributions of PEO at a lower density ~ 0.5 g/cm^3 again suggest the loose and brushy nature of the PEO corona. Next we compute the average radius of the micellar core R_c, which can be defined as the distance between PS-PEO interface and the center of the worm micelle. Variation of R_c along the central axis of the worms are shown in **Figure 2C** averaged over 600 ns. In agreement with experiment, the jagged nature of the hydrophobic backbone of both the worm micelles is clearly evident. This agrees well with highly stable and glassy nature of the PS core.

After characterizing the worm structure, FRAP experiments are performed to study the mobility of PKH26 hydrophobic dye molecules within the core of the micelle. No significant fluorescence recovery is seen up to 20 minutes with OS90 worms when all chloroform has been evaporated from the core (**Figure**

3A). For typical flexible diblock worm micelles with fluid cores, the FRAP recovery time is of the order of seconds, indicating the OS90 core is very highly entangled and glassy, preventing even the mobility of a small embedded dye molecule. FRAP on the aqueous OS30 worms also confirms the glassiness of the worm backbone. Temperature dependent FRAP also shows no clear indication of breaking glassiness up to 60 ^{o}C (See **Supplemental Information**).

While the PS core is glassy, the loose PEO corona is more fluid-like. The combined effect can determine the overall rigidity of the worm. Now, to characterize the polymer segmental relaxation within the worm micelle, we also calculate self-intermediate scattering function ($F_s(Q,t)$)[53] of PEO and PS for the simulated worms. These calculations are averaged over the center of mass of each PEO and PS chains separately and over different reference initial times. Results are shown in **Figure 3B**. Much faster relaxation of $F_s(Q,t)$ of PEO compared to PS indicates the time scale difference between corona and core regions of the worm. To estimate the time scale difference more quantitatively, we fit the decay curves using a Kohlrausch-Williams-Watts (KWW) multi-stretched exponential[54, 55] and calculate average relaxation times ($\tau(Q)$). Compared to PEO (τ_{PEO} ~2 ns), the average relaxation time of PS (τ_{PS} ~50 ns) is nearly 25 times longer. Next, to investigate the polymer diffusion in more detail, we calculate MSD ($<\Delta r^2>$) of PEO and PS center of mass, as shown in **Figure 3C**. At short time scales, polymers generally follow Rouse dynamics[33, 56, 57]. We fit the MSD data with a power low ($<\Delta r^2> = t^{\alpha}$ where α is the exponent). α value lower than the unit clearly reveals the sublinear diffusion of both PEO and PS. Much lower α value indicates more sublinear diffusion for PS (0.48) compared to PEO (0.77). The entanglement molecular weight of PS at room temperature of ~ 160 monomers is much longer than the length of the hydrophobic tails. At 353 K, the entanglement molecular weight of PEO ~ 44 monomers[58], which is approximately the length of the hydrophilic PEO in our simulations. Here, α for PS ~ 0.48 is consistent with Rouse dynamics.

Solvent Effect So far it is clear that PS based diblock copolymers provide stable and rigid worm micelles. The high glass transition temperature of the PS core makes the PS-based worm micelle very rigid over a range of temperatures. While temperature has very little effect, addition of organic solvent can alter the rigidity of the worm due to the breaking of glassiness of the PS core. Thus, specific solvent can be easily used to engineer worm micelles with controlled flexibility. To study this, various organic solvents, in 1 µl or 0.5 µl increments, are added to a 1 ml solution of 0.1 mg/ml OS30 during the hydration step. The solvent was retained in the hydrophobic core (and solution) without evaporation, and the effects of increasing solvent on the worm yield and contour length of the OS30 system was studied. The contour length was measured as the average of at least 10 worms**.** Three solvents, chloroform, toluene and xylene were chosen to be the hydrophobic core fluidizers. Importantly, the presence of solvent not only fluidized the PS core but also changed the shape of the worm to vesicles and spherical micelles. A rough estimate of the percentage of worms in solution is obtained by counting the number of worms among the population containing worms, vesicles and spherical micelles for up to 7 randomly selected areas of the sample chamber (521x512 pixel frames at 60X magnification). Adding chloroform in increasing quantities during hydration does not affect the glassiness of the OS30 worms until around 1% chloroform. At these higher concentrations, the glassiness and hinged morphologies vanish, with the worms becoming smooth and increasingly flexible. Across the entire range of chloroform concentrations tried, the worms have a remarkably consistent contour length of around 12 µm, with a less than 10% population of spherical morphologies (**Figure 4A**). Toluene, on the other hand, produces a mixture of spherical morphologies and stiff, hinged worms until a concentration of 0.26%. At higher concentrations the worms become flexible, and giant vesicles are found to co-exist with the worms and spherical micelles. The giant vesicles are easily identified by the edge brightness created by the bi-layered structure. Both the contour length of the worms and the fraction of worms in the population show a peaking behavior at the concentration of toluene at which the worms become flexible (**Figure 4B**). At higher concentrations of toluene (> 0.4%), the worm fraction is so low and the worms become so soft that their disintegration into spherical micelles can be seen under the microscope. This observation warrants a time-course study of the solvent saturated systems to systematically monitor any morphological changes over time. Xylene breaks the glassiness of the OS30 worms at a very small concentration (< 0.1%), and has a consistently increasing fraction of giant vesicles. While the length distribution is found to be unchanged **(Figure 4C**), the worms are found to become increasingly more flexible with the increasing concentration of xylene.

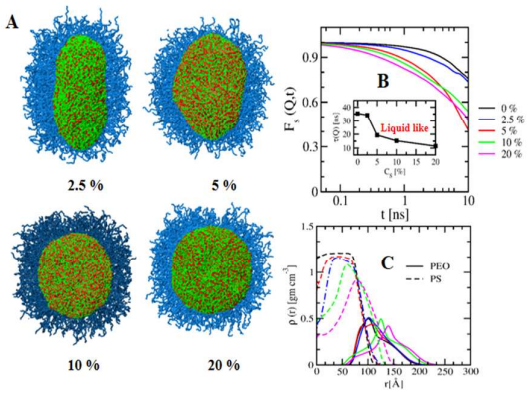

Fig 6(A) Final snapshots of OS30 after 50 ns simulation in presence of model hydrophobic solvent of four different concentrations. (B) $F_s(Q,t)$ of PS monomers in presence of model hydrophobic solvent at four different concentrations. Variation of average relaxation time, τ (Q), as function of solvent concentration is shown in the inset. (C) Density profile of PEO (solid line) and PS (dotted line) in worm-like morphology relative to the center of mass of the worm core in presence of hydrophobic solvent at different concentrations.

The observation of worm disintegration into spherical micelles in the soft toluene system prompted a time-based study of the soft worms with the various solvents in the core. Three samples of flexible OS30 worms are prepared with 1.2 % chloroform, 0.5 % toluene and 0.5 % xylene respectively. Over a course of two days, the toluene contour length distribution decreases steadily from 10 ± 3 μm to being centered on 5 ± 3 μm (**Figure 5A**). A noticeable increase in the number of spherical micelles and giant vesicles is also observed. Xylene worms maintained their length distributions over a period of two days, with no significant change in the fraction of different morphologies. The persistence length averaged over 12-15 worms was also found to be remarkably consistent over this time period (**Figure 5**). The persistence length l_p was obtained by numerical fitting to the relation

$$\langle R^2 \rangle = 2l_p^2[L/l_p - 1 + \exp(-L/l_p)]$$

Where R is the end-to-end distance of the worm, and L is the contour length. Chloroform solvated worms show a slight increase in the contour length and a dramatic increase in the persistence length over two days. At the end of 48 hours, the worms regained their glassiness and hinged dynamics, and the tangent-tangent correlation method had to be used to calculate the persistence length. The high vapor pressure of chloroform allows it leave the solution easily into the air column in the sample vial. This might be the reason why the worms to stiffen over time.

The threshold concentration needed to form worms is plotted as a function of solubility of the corresponding organic solvents in water in **Figure 4D**. The linear relation indicates that the threshold concentration is representative of the partition coefficient of the solvent into the worm-core in the worm-water system. Of the three solvents, chloroform has the highest solubility in water, followed by toluene and xylene. Thus a higher concentration of chloroform is needed before it can fluidize the worm core by partitioning into it. Chloroform also having the highest vapor pressure, leaves the solution into the air the fastest, leading to the increasing stiffness of worms with time. Toluene and xylene are cyclic molecules, similar in structure to styrene, and hence are extremely good solvents for polystyrene. The softening and breaking up of OS30 worms in the presence of excess toluene most likely indicates an enhanced mobility of the polystyrene chains resulting in breaches in the core-corona boundary, and possible recruitment of the PS-PEO chains to stabilize solvent droplets. Xylene is found to be an ideal solvent for PS in the context of the current experiments. The extremely low solubility of xylene in water results in fairly stable populations of worms and vesicles over a period of a few days, and a controlled softening of both the OS30 and OS90 worms is demonstrated.

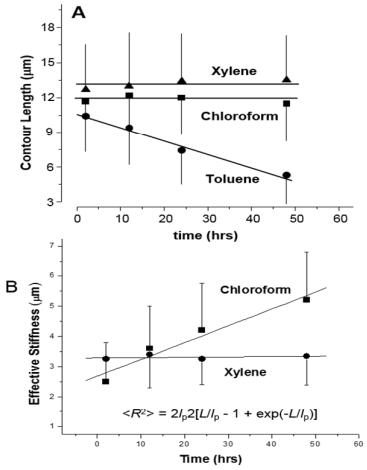

Fig 5 (A) Stability of OS30 worms with solvents in core. Flexible worm samples were prepared with 1.2 % chloroform, 0.5 % toluene and 0.5 % xylene, and observed for a period of two days. (A). The contour lengths of the chloroform and xylene containing worms are constant while the toluene worms shorten steadily. An increase in the population of vesicles and spherical micelles is observed for the toluene system. (B). The persistence length of the worms is measured in the semi-flexible regime approximation. Xylene containing worms are robust and maintain a uniform persistence length over two days. Chloroform worms stiffen steadily, eventually becoming hinged and glassy again after 2 days.

A similar shape change often happens after loading drug or guest molecule inside worm micelles and is closely related to its loading efficiency[49]. Hence, PEO-PS worms can be a very good model system to study the shape transformation of worm micelles in the presence of small guest molecules. A number of theories already exist regarding the shape change of polymer aggregates in the presence of guest molecules. They are mostly based on the mean field approximation[32]. To the best of our knowledge, no MD simulation studies have been performed so far to characterize the transformation of worm micelles to spherical micelles. Now, to explore the shape change of the micelle computationally, we simulate OS30 in the presence of 2.5%, 5%, 10%, and 20% model hydrophobic solvent. Before going to any further detail, it is important to mention here that like experiment, we are not exploring the role of any specific organic solvents like chloroform or

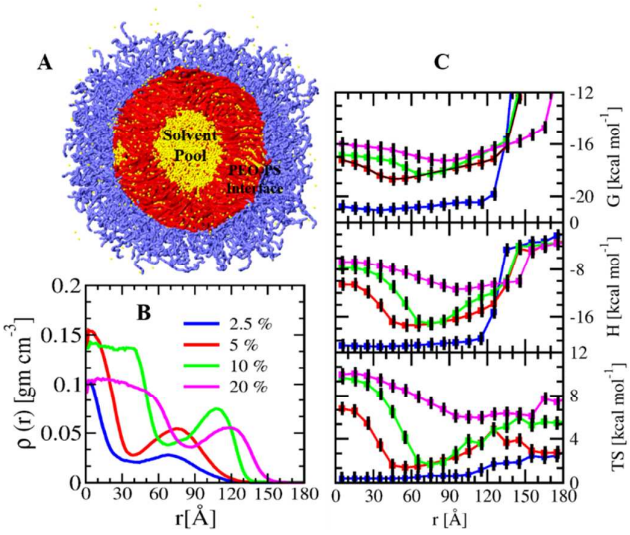

Fig 7 (A) Distribution of hydrophobic solvent within the worm. Here solvent is shown in yellow color and PEO and PS in blue and red color respectively. (B) Density profile of hydrophobic solvent relative to the center of mass of the worm. (C) Thermodynamic properties of hydrophobic solvent as a function of distance from the central axis of PEO-PS worm micelle (including error).

xylene or toluene. The main focus of this simulation study is to understand the role of solvent or small organic molecules in general. The final snapshots of the worm after 50 ns in presence of model solvent at four different concentrations are shown in **Figure 6A**. For 2.5 % solvent, the shape of the worm remains almost same. However, with increasing the solvent concentration, the worm core starts to change its shape and eventually forms a spherical micelle in the presence of 10 % or higher solvent. Without hydrophobic solvent, the glassy nature of the PS core makes the PEO-PS worm micelle very stable. Hydrophobic solvents most likely fluidize the core and transform the worm micelle to spherical micelle. Now, to explore the PS dynamics in presence of hydrophobic solvent, we calculate $F_s(Q,t)$ of each PS monomer. The relaxation patterns of $F_s(Q,t)$ for different solutions are shown in **Figure 6B**. The average relaxation times ($\tau(Q)$) are also incorporated into the inset of the figure. With increasing solvent concentration, the correlation function relaxes much faster, especially after 5 % solvent, indicating the fluid-like nature of the worm core. A sudden decrease in the average relaxation time after 5 % hydrophobic solvent is also evident. This indicates that due to the likely glassy nature of the hydrophobic core in the presence of 2.5 % solvent, the structure of the worm micelle remains stable. As we further increase the solvent concentration, the worm core becomes more fluid-like and the shape of the worm micelle shifts. Hence, even for model hydrophobic solvent a threshold amount of solvent is essential to shift the shape as well as the rigidity of the worm micelle. This agrees well with experimental findings. The change in density profiles for both PEO and PS also reveal the shape change of the worm core in presence of hydrophobic solvent, as shown in **Figure 6C**. With increasing hydrophobic solvent concentration, the PEO peak position shifts to a higher value, especially at 10 % or higher solvent concentration. This demonstrates that in the presence of organic solvent, the PEO-PS worm micelle transforms to a spherical shape with a larger core radius. We find that the radius of the core scales with the concentration of solvent, (**see SI 3C**). Our data also reveals that like PEO, the density profile of PS also depends on solvent concentration. At the very center of the worm due to the accumulation of organic solvent, PS density decreases with increasing solvent concentration **(see SI 4),** $\rho_{max} \sim C_s^{-.126}$**.** Furthermore, the interfacial width increases with the concentration of solvent, $D_w \sim C_s^{0.36}$ (see **SI 3D**), most likely due to a lowering of the interfacial tension[59].

From the above, we can infer that the free energy of the micelle system shifts due to the free energy of dilution of the hydrophobic block, PS, which consists of the entropy and enthalpy of mixing with the organic solvent[32]. In addition, the free energy of the interface is shifting as a function of increased solvent concentration. These results are consistent with analytic calculations using the mean field approximation by Nagarajan[32]. Next, it is interesting to characterize the distribution of hydrophobic solvent inside the worm. The solvent distribution for 10%, as well as for all other concentrations are shown in **Figure 7A** and **SI 6** respectively. Two different types of solvent distributions at high and low solvent concentration are clearly visible. To begin with, for 2.5% solvent, both the solvent and PS coexist inside the worm core without any separation between them suggesting the structure is more analogous to a simple solubilization model. As the concentration of solvent increases further, the mobile solvent phase and relatively rigid hydrophobic polymer phase start to separate with the formation of pure 'solvent pool' in the center of the worm core. With increase of solvent concentration, the size of the pool quickly expands and eventually transforms the worm micelle to a spherical micelle. As both the solvent and PS remain completely miscible without formation of any pure solvent pool in the center of the worm for 2.5% solution, the shape of the aggregate changes very little. On the other hand, at high concentration, the solvent molecules form a pure solvent pool in the center of the worm and transform it into a spherical micelle. Previously Nagarajan[32] also studied the stability of polymer micelles in the presence of hydrophobic solubilizer based on the mean field approximation. In their approximations, the polymer micelle with a zero pure solubilizate pool was found to be free energetically most stable. In our case, the formation of a solvent pool is evident from the density distributions of hydrophobic solvent from the central axis of the worm (**Figure 7B**). The distributions show two peaks near the center and the interface between PEO and PS irrespective of solvent concentration. At higher concentration, the peak near the center broadens again

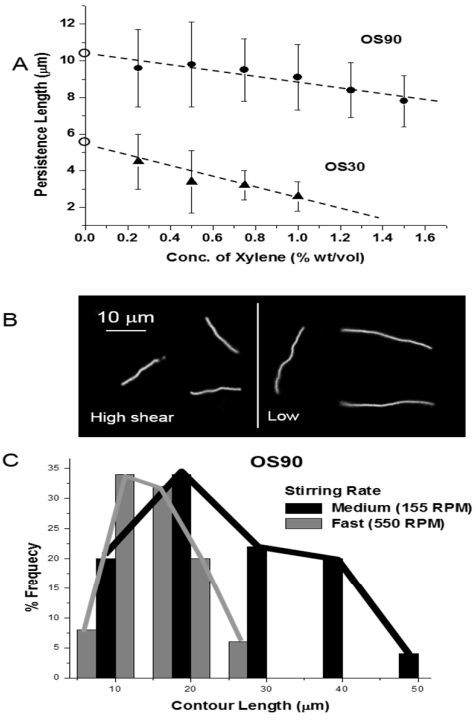

Fig 8 Engineering worm micelles. (A). The tunable flexibility of the solvent softening OS system is demonstrated. Adding increasing amounts of xylene makes the worms increasingly flexible. At less than 1% concentrations both the OS30 and OS90 systems are stable for up to two weeks. The persistence lengths of the glassy worms are shown by the hollow circles. (B). The normally long and convoluted OS90 worms can be straightened and shortened by stirring the sample during the solvent evaporation step.The average straightness ratio Lee/Lc (Lee is the end to end distance, Lc is the contour length) for OS90 worms is 0.4. It increases to 0.75 and 0.91 when the worms are stirred at a medium and fast rate respectively. (C). The change in size distribution upon stirring is plotted. The stirring rates are nominal values for a 400 ml top load of water in a 600 ml pyrex

indicating the presence of a hydrophobic solvent pool inside the worm.

Hence, depending on the distributions of the hydrophobic solvent inside the worm core, two different types of structures are clearly visible. At lower concentration of model solvent, the structure is more analogous to a simple solubilization model without any localization of the solvent inside the worm core. With increasing solvent concentration, a microscopic phase separation occurs between the model solvent and PS inside the worm. The structure of the aggregate changes to a droplet microemulsion with a pure solvent pool in the center. Formation of such a solvent pool in the center results in the transformation of the worm to spherical micelle. Next, to understand the phase separation between solvent and polymer in more detail herein we calculate thermodynamic properties of the hydrophobic solvent using the 'SPAM' method, originally used to calculate the relative free energy of water around biomolecules[51]. A detailed description of the methodology can be found in the methods section. The SPAM method allows us to calculate the free energy of the solvent present at different regions of the worm core without doing any additional biased simulations. Free energy, entropy and enthalpy of the hydrophobic solvent as a function of distance from the central axis of the worm are shown in **Figure 7C**. The entropy and enthalpy of the hydrophobic solvent are the entropy of mixing with the PS and the enthalpy of mixing with the PS, respectively. In 2.5 % solvent, the energy profile is almost flat without any minima. As the solvent concentration increases (5% or higher), the free energy profile shows one minima near the PEO-PS interface. But with further increasing the solvent concentration (20 %), the minimum becomes less deep or flatter. Like free energy, entropy and enthalpy of the solvent also show no minimum near the PEO-PS interface for 2.5 % solvent. This reveals that at lower concentration the solvent enthalpy of mixing with the PS is high but entropy of mixing with the PS is low (nearly zero). This agrees well with the solubilization model structure of the polymer aggregate. For 2.5 % solution the worm core still remains glassy and highly packed. As the core is densely packed, the solvent mixing enthalpy with the PS is low, but the mixing enthalpy is high due to strong interactions with neighboring PS molecules. Thus, at lower concentrations, accumulation of hydrophobic solvent inside the worm core is an enthalpy driven process, promoted by the enthalpy of mixing with the PS, and the structure of the aggregate is more analogous to a simple solubilization model. As we increase the concentration, the worm core becomes more fluid-like and the organic solvent starts to form a hydrophobic pool near the central region of the worm, decreasing the PS density of the core, increasing the hydrophobic core size resulting in the overall shape of the worm shifting to a spherically symmetric micelle. Inside the 'pool', the entropy of the solvent mixing with the PS is higher (due to greater free volume) but near the PEO-PS interface, the enthalpy of mixing with the PS is more negative (due to strong interaction of solvent with densely packed PS). As a result, at 5% and higher solvent concentration, the solvent density profile displays two peaks, one near the center in the hydrophobic 'pool' and one at the PEO-PS interface. Thus, the accumulation of hydrophobic solvent inside the worm core at higher concentrations, is a combination of both enthalpic and entropic effects of the interaction of the PS with the solvent. The energy cost for pool formation due to the replacement of PS from the central region of the worm core is compensated by the entropy gain of the organic solvent present inside the hydrophobic pool at higher concentration. With even further increase of solvent concentration, both the 'pool' size and core radius increase while the worm core becomes more loosely packed. As a result, solvent entropy increases further but enthalpy decreases and the minima near the PEO-PS interface starts to disappear. This suggests that at very high concentration the solvent accumulation process inside the worm is an entropy driven process. Saito *et al.*[60] have also reported that the solubilization of estriol, a drug molecule, in a triblock copolymer is mainly governed by entropy change of the drug. Eventually, the solvent entropy becomes high enough to break the PEO-PS assembly. This accumulation of solvent correlates with a lowering of the interfacial tension due to solvent accumulation at the interface. Thus, our free energy analysis shows, how dependent on solvent concentration, entropic and enthalpic effects of the solvent interacting with the PS can change the shape of the worm micelle. From experiments it is found that compared to toluene or xylene (more hydrophobic), the worm-like morphology of OS30 remains stable in a more concentrated chloroform (less hydrophobic). Due to their more hydrophobic nature, Toluene and Xylene may prefer the central region of the worm more than the PEO-PS interface and can change the shape of the worm more effectively than Chloroform.

Engineering worm shape and stiffness Xylene is found to be an ideal solvent to create worms with tunable stiffness. The tunable flexibility of the OS30 and OS90 worms with xylene in their core is shown in **Figure 8**. The OS30 system is stable and consistent for at least 2 days, and for the lower concentrations of xylene, up to 2 weeks at room temperature. The higher concentrations of xylene in OS30 tend to induce vesicle formation after about 3-4 days, whereas the higher molecular weight OS90 retains the worm fraction for at least two weeks. By projecting the curve it is seen that at about 1.5 % xylene, the OS30 system has a vanishingly small persistence length, which corresponds to the projection of the solvent effects plot (**Figure 4C**) where the fraction of worms is very small and the system consists entirely of giant vesicles and some spherical micelles.

The OS90 worms possess an average straightness ratio (L_{ee}/L_c, where L_{ee} is the end to end distance, and L_c is the contour length) of 0.4. Looking at the shapes of the locked in curvature of the glassy worms, we hypothesized that one could engineer the shapes of the worm backbone by controllably evaporating the solvent during the worm formation process. To this end, 2% chloroform in water solution was added to a thin film of OS90 copolymer and the excess chloroform was evaporated out in a controlled manner using a stir bar spinning at two different steady rates. At 155 RPM spinning for 1 hour, the distribution of worm lengths was similar to that of an unstirred system, but the worms were much straighter with the average straightness ratio (L_{ee}/Lc) of about 0.75. For spinning at setting 550 RPM, the contour length distribution shifted dramatically to shorter lengths, and the average straightness ratio was 0.91. This simple and rough experiment proves that the worm morphology can be engineered by controlling the shear and evaporation conditions during the solvent evaporation step.

The persistence length l_p can be related to the interfacial tension as well as the diameter of the core. For a D^*-dimensional object the rigidity is $\boldsymbol{\kappa = \Phi \gamma d_c^{4-D^*} \sim l_p k_B T}$, in which Φ is an interfacial coupling constant, γ is the interfacial tension, and d_c is the diameter of the hydrophobic core[61]. The interfacial coupling constant $\boldsymbol{\Phi \approx 0.05}$ is found for cylindrical block copolymer filomicelles [61]. In our case, D^* = 1. Based on simulation results as discussed within, we find that while the core diameter increases, the interfacial width widens, and thus the interfacial tension decreases. The decrease in persistence length may be primarily attributed to this effect, as well as the decrease in glassy hydrophobic PS density in the core.

Conclusions

PS-PEO worms form a novel class of worms that are extremely rigid with a frozen-in curvature. Extraordinarily slow mobility of embedded dye indicates the glassy nature of the hydrophobic worm core. The mobility of embedded dye molecules is extremely low even at 60 °C suggesting there is no lowering of glass transition temperatures for PS in the worm configuration. While temperature has little effect, addition of block specific solvents dramatically alters the characteristics of the worms, fluidizing them and even favoring non-worm like morphologies. Xylene is seen to be a particularly useful solvent as it is possible to controllably affect the stiffness of the worms by changing the concentration of added xylene. Within the worm micelle, we find that organic solvent accumulates both at the hydrophobic/hydrophilic interface and also in the center of the worm micelle core. Thus, control of the worm diameter as well as the width of the interface through addition of organic components can be used as a method to engineer worm micelles with controlled flexibility. This opens up enormous possibilities for using these self-assembled rods as super high aspect ratio colloidal systems or as nanocarriers with specified rigidity.

Conflicts of interest

"There are no conflicts to declare".

Acknowledgements

This research was supported, in part, by the NSF through XSEDE resources under grant number TG-CHE130099 and a grant of computer time from the City University of New York High Performance Computing Center under NSF Grants CNS-0855217, CNS-0958379 and ACI-1126113. S.M.L. acknowledges start-up funding received from College of Staten Island and City University of New York. S.M.L. would also like to acknowledge PRF 54235-DNI6 and NSF 1506937 for support.

References

1. L. F. Zhang and A. Eisenberg, *Science*, 1995, **268**, 1728-1731.
2. D. E. Discher and A. Eisenberg, *Science*, 2002, **297**, 967-973.
3. S. Jain and F. S. Bates, *Science*, 2003, **300**, 460-464.
4. P. Dalhaimer, A. J. Engler, R. Parthasarathy and D. E. Discher, *Biomacromolecules*, 2004, **5**, 1714-1719.
5. Y. Geng, P. Dalhaimer, S. S. Cai, R. Tsai, M. Tewari, T. Minko and D. E. Discher, *Nature Nanotechnology*, 2007, **2**, 249-255.
6. S. Li, B. Byrne, J. Welsh and A. F. Palmer, *Biotechnol Prog*, 2007, **23**, 278-285.
7. D. Discher, in *Introduction to Nanoscale Science and Technology*, ed. S. E. a. J. H. Massimiliano Di Ventra, Springer US, 2006.
8. J. S. Qian, M. Zhang, I. Manners and M. A. Winnik, *Trends in Biotechnology*, 2010, **28**, 84-92.
9. P. Bhargava, Y. Tu, J. X. Zheng, H. Xiong, R. P. Quirk and S. Z. Cheng, *J Am Chem Soc*, 2007, **129**, 1113-1121.
10. H. G. Cui, Z. Y. Chen, S. Zhong, K. L. Wooley and D. J. Pochan, *Science*, 2007, **317**, 647-650.
11. K. Rajagopal, A. Mahmud, D. A. Christian, J. D. Pajerowski, A. E. X. Brown, S. M. Loverde and D. E. Discher, *Macromolecules*, 2010, **43**, 9736-9746.
12. C. J. Ellison, R. L. Ruszkowski, N. J. Fredin and J. M. Torkelson, *Physical Review Letters*, 2004, **92**.
13. C. J. Ellison, M. K. Mundra and J. M. Torkelson, *Macromolecules*, 2005, **38**, 1767-1778.
14. R. D. Priestley, C. J. Ellison, L. J. Broadbelt and J. M. Torkelson, *Science*, 2005, **309**, 456-459.
15. Y. Chai, T. Salez, J. D. McGraw, M. Benzaquen, K. Dalnoki-Veress, E. Raphael and J. A. Forrest, *Science*, 2014, **343**, 994-999.
16. Z. H. Yang, Y. Fujii, F. K. Lee, C. H. Lam and O. K. C. Tsui, *Science*, 2010, **328**, 1676-1679.
17. M. K. Mundra, C. J. Ellison, P. Rittigstein and J. M. Torkelson, *Eur Phys J-Spec Top*, 2007, **141**, 143-151.
18. Y. Rharbi, *Physical Review E*, 2008, **77**.
19. C. Zhang, Y. L. Guo and R. D. Priestley, *Macromolecules*, 2011, **44**, 4001-4006.
20. T. Sasaki, A. Shimizu, T. H. Mourey, C. T. Thurau and M. D. Ediger, *Journal of Chemical Physics*, 2003, **119**, 8730-8735.
21. J. F. Ding, G. Xue, Q. P. Dai and R. S. Cheng, *Polymer*, 1993, **34**, 3325-3327.
22. U. Gaur and B. Wunderlich, *Macromolecules*, 1980, **13**, 1618-1625.
23. M. M. Mok and T. P. Lodge, *Journal of Polymer Science Part B-Polymer Physics*, 2012, **50**, 500-515.
24. E. Q. Chen, Y. Xia, M. J. Graham, M. D. Foster, Y. L. Mi, W. L. Wu and S. Z. D. Cheng, *Chemistry of Materials*, 2003, **15**, 2129-2135.
25. L. F. Zhang and A. Eisenberg, *Journal of Polymer Science Part B-Polymer Physics*, 1999, **37**, 1469-1484.
26. J. Grandjean and A. Mourchid, *Europhys Lett*, 2004, **65**, 712-718.
27. L. Liu, Gao, X., Cong, Y., Li, B., Han, Y., *Macromolecular Rapid Communications*, 2006, **27**, 260-265.
28. R. H. Deng, M. J. Derry, C. J. Mable, Y. Ning and S. P. Armes, *Journal of the American Chemical Society*, 2017, **139**, 7616-7623.
29. Q. Chen, H. Schonherr and G. J. Vancso, *Small*, 2010, **6**, 2762-2768.
30. D. A. Wilson, R. J. M. Nolte and J. C. M. van Hest, *Nature Chemistry*, 2012, **4**, 268-274.
31. H. L. Che and J. C. M. van Hest, *Journal of Materials Chemistry B*, 2016, **4**, 4632-4647.

32. R. Nagarajan, *Polymers for Advanced Technologies*, 2001, **12**, 23-43.
33. K. Kremer and G. S. Grest, *Journal of Chemical Physics*, 1990, **92**, 5057-5086.
34. R. J. Lang, W. L. Merling and D. S. Simmons, *Acs Macro Letters*, 2014, **3**, 758-762.
35. A. Shavit and R. A. Riggleman, *Journal of Physical Chemistry B*, 2014, **118**, 9096-9103.
36. V. A. Harmandaris, N. P. Adhikari, N. F. A. van der Vegt and K. Kremer, *Macromolecules*, 2006, **39**, 6708-6719.
37. F. Varnik, J. Baschnagel and K. Binder, *Physical Review E*, 2002, **65**.
38. K. Yoshimoto, T. S. Jain, K. V. Workum, P. F. Nealey and J. J. de Pablo, *Physical Review Letters*, 2004, **93**.
39. G. Milano and F. Muller-Plathe, *Journal of Physical Chemistry B*, 2005, **109**, 18609-18619.
40. H. A. Harimi-Varzaneh, N. F. A. van der Vegt, F. Mueller Plathe and P. Carbone, *ChemPhysChem*, 2012, **13**, 3428-3439
41. M. Drenscko and S. M. Loverde, *Molecular Simulation*, 2017, **43**, 234-241.
42. D. Fritz, C. R. Herbers, K. Kremer and N. F. A. van der Vegt, *Soft Matter*, 2009, **5**, 4556-4563.
43. G. Rossi, L. Monticelli, S. R. Puisto, I. Vattulainen and T. Ala-Nissila, *Soft Matter*, 2011, **7**, 698-708.
44. W. Shinoda, R. DeVane and M. L. Klein, *Molecular Simulation*, 2007, **33**, 27-36.
45. X. Periole and S. Marrink, in *Biomolecular Simulations: Methods and Protocols*, ed. L. M. a. E. Salonen, Springer, New York, 2013, vol. 294, pp. 533-565.
46. W. Shinoda, R. DeVane and M. L. Klein, *Journal of Physical Chemistry B*, 2010, **114**, 6836-6849.
47. R. DeVane, W. Shinoda, P. B. Moore and M. L. Klein, *Journal of chemical theory and computation*, 2009, **5**, 2115-2124.
48. W. Shinoda, R. DeVane and M. L. Klein, in *Coarse-Graining of Condensed Phase and Biomolecular Systems*, ed. G. A. Voth, CRC Press, 2008, ch. 22, pp. 329-342.
49. S. M. Loverde, M. L. Klein and D. E. Discher, *Advanced materials*, 2012, **24**, 3823-3830.
50. S. Plimpton, *Journal of Computational Physics*, 1995, **117**, 1-19.
51. G. Cui, J. M. Swails and E. S. Manas, *Journal of chemical theory and computation*, 2013, **9**, 5539-5549.
52. S. M. Loverde, V. Ortiz, R. D. Kamien, M. L. Klein and D. E. Discher, *Soft Matter*, 2010, **6**, 1419-1425.
53. J. P. Hansen and I. R. McDonald, *Theory of Simple Liquids*, Elsevier, 1990.
54. F. Kohlrausch, *Pogg. Ann. Phys.*, 1863, **119**, 352.
55. G. Williams and D. C. Watts, *Transactions of the Faraday Society*, 1970, **66**, 80-+.
56. P.-G. De Gennes, *Scaling concepts in polymer physics.*, Cornell university press., 1979.
57. M. Doi, & Edwards, S. F. , *Theory of Polymer Dynamics.*, Oxford University Press., 1988.
58. A. N. Semenov and M. Rubinstein, *European Physical Journal B*, 1998, **1**, 87-94.
59. J. Noolandi and K. M. Hong, *Macromolecules*, 1983, **16**, 1443-1448.
60. Y. Saito, Y. Kondo, M. Abe and T. Sato, *Chemical and Pharmaceutical Bulletin*, 1994, **42**, 1348-1350.
61. P. Dalhaimer, F. S. Bates and D. E. Discher, *Macromolecules*, 2003, **36**, 6873-6877.